

Generating 10–40 MeV high quality monoenergetic electron beams using a 5 TW 60 fs laser at Tsinghua University*

HUA Jian-Fei(华剑飞)¹ YAN Li-Xin(颜立新) PAI Chih-Hao(白植豪) ZHANG Chao-Jie(张超杰)
LI Fei(李飞) WAN Yang(万阳) WU Yi-Peng(吴益鹏) XU Xin-Lu(徐新路) DU Ying-Chao(杜应超)
HUANG Wen-Hui(黄文会) CHEN Huai-Bi(陈怀璧) TANG Chuan-Xiang(唐传祥) LU Wei(鲁巍)

Department of Engineering Physics, Tsinghua University, Beijing 100084, China

Abstract: A unique facility for laser plasma physics and advanced accelerator research has recently been built at Tsinghua University. This system is based on a Tsinghua Thomson scattering X-ray source (TTX), which combines an ultrafast TW laser with a synchronized 45 MeV high brightness linac. In our recent laser wakefield acceleration experiments, we have obtained 10–40 MeV high quality monoenergetic electron beams by running the laser at 5 TW peak power. Under certain conditions a very low relative energy spread of a few percent can be achieved. Absolute charge calibration for three different scintillating screens has also been performed using the linac system.

Key words: laser-plasma accelerator, monoenergetic, electron charge

PACS: 52.38.Kd, 52.59.Bi, 41.75.Jv **DOI:** 10.1088/1674-1137/39/1/017001

1 Introduction

Plasma acceleration based on the wakefield concept [1, 2] has made great strides in the past decade. By utilizing table-top 10 TW-PW laser systems, high quality monoenergetic electron beams with energies of up to few GeV [3–9] and an energy spread of a few percent [10–12] have been obtained worldwide. In this paper, we report our recent experimental results on laser plasma acceleration utilizing a newly built facility at Tsinghua University. This facility is based on the Tsinghua Thomson scattering X-ray source (TTX) [13, 14], which combines an ultra-fast TW Ti:sapphire laser system with a synchronized 45 MeV high brightness linac. By running the laser at 5 TW 60 fs, high quality 10–40 MeV monoenergetic electron beams have been obtained. In addition, under certain plasma conditions, a very low relative energy spread of a few percent has been achieved. This paper is organized as follows: in Section 2, the facility will be briefly overviewed; in Section 3, the experimental results will be presented in detail; and, a summary is provided in Section 4.

2 Overview of the Tsinghua laser plasma acceleration platform

The laser plasma acceleration platform at Tsinghua

University has three major components: the TW laser system, the 45 MeV high brightness linac, and an experimental system combining a high vacuum chamber with a set of various optical and electric diagnostics. We will next describe these subsystems in detail.

2.1 TW laser system

The TW laser system (Fig. 1), which is based on the standard CPA (Chirped Pulse Amplification) and MOPA (Master Oscillator Power Amplifier) architecture, has six major components: an oscillator, a stretcher, a regenerative amplifier, two multi-pass amplifiers, and a vacuum compressor [15].

The 20 fs Ti:sapphire oscillator with a rep-rate of 79.3 MHz is pumped by a frequency-doubled YVO₄ laser (Verdi-5). A fused-silica prism pair is used for intracavity dispersion compensation. Synchronization between the oscillator and the RF signal is achieved by a piezoelectric transducer (PZT) based feedback loop, with a timing jitter less than 200 fs. Before entering the regenerative amplifier, the seed pulse goes through a Pockels cell pulse selector and is then stretched to about 300 ps with a modified offener type stretcher. In the regenerative amplifier pumped by a frequency-doubled Q-switched Nd:YLF laser (Evolution-30), the laser pulse is amplified to about 3 mJ, with a rep-rate of 1 kHz, and the bandwidth is reduced to 25 nm. Another Pockels cell pulse cleaner is in-

Received 20 January 2014

* Supported by NSFC (11375006, 11005063, 11175102), Tsinghua University Initiative Scientific Research Program, the Thousand Young Talents Program and Beijing Higher Education Young Elite Teacher Project

1) E-mail: jfhua@tsinghua.edu.cn

©2015 Chinese Physical Society and the Institute of High Energy Physics of the Chinese Academy of Sciences and the Institute of Modern Physics of the Chinese Academy of Sciences and IOP Publishing Ltd

serted before the first multi-pass amplifier to enhance the laser contrast against the ns prepulse and ASE. In the first four-pass amplifier pumped by frequency-doubled Q-switched Nd: YAG lasers (Quanta-Ray Pro-350), the pulse is amplified to 100 mJ in a bow-tie configuration. The laser beam is then split into two beams: one beam (70 mJ) is a seed for the final amplifier and the other beam (30 mJ) is used for third-order harmonic generation to drive the RF photocathode gun.



Fig. 1. The ultrashort high power laser system at Tsinghua University.

The final amplifier is another four-pass bow-tie amplifier pumped with two frequency-doubled Q-switched Nd:YAG lasers (Saga 230) from both ends. The amplification media is a 20 mm-long, 20 mm-diameter, normal-cut Ti:sapphire crystal with anti-reflective coating. With a combined pump energy of 2.8 J, the laser pulse can be amplified to 1.0 J. A computer-controlled energy tuner made of a half-wave plate and a thin-film polarizer is utilized to adjust the laser pulse energy before compression. The laser pulse is expanded to 50 mm-diameter beam size and it is then sent into the vacuum compressor. After compression, about 70% of the laser energy can be sent into the experimental system. The final energy on target can reach up to 500 mJ, after taking into account the losses on transmission.

For laser-plasma interaction experiments, the three crucial parameters are: laser temporal contrast, focal spot quality and pulse duration. High temporal contrast is needed to avoid pre-plasma ionized by prepulses. A high quality focal spot helps to excite the stable wake and to increase the energy coupling. Pulse duration should be compressed to as short as possible to increase the peak laser power. Thanks to significant efforts in the past few years, our laser system has been thoroughly optimized for wakefield experiments. The typical parameters of our laser are listed in Table 1.

The contrast at the nanosecond is measured by a fast photodiode coupled with ND filters, and the contrast at the picosecond is measured by a commercial third-order autocorrelator. The contrast has also been verified through experiments by observing pre-plasma using interferometry. At laser peak power, we have found no

pre-plasma when scanning the delay time between the main laser pulse and the probe pulse. To further enhance the contrast, a technology called cross-polarized wave (XPW) generation has been tested, and a contrast enhancement of 2–3 orders at ps time has been confirmed, as shown in Fig. 2.

Table 1. The parameters of TW laser system.

laser parameters	value
central wavelength/nm	800
pulse duration/fs	60–70
repetition rate/Hz	10
energy on target/mJ	500
energy stability(%)	1.5
contrast ratio	$8.1 \times 10^6 @ 10$ ns
	$1.9 \times 10^5 @ 10$ ps
	$2.5 \times 10^4 @ 1$ ps
focus spot (FWHM) ^{1)/} μm	16.6 (horizontal)
	12.3 (vertical)
pointing stability (rms)/ μrad	4.5 (horizontal)
	5.3 (vertical)

1) Measured with an OAP mirror of 500 mm focal length.

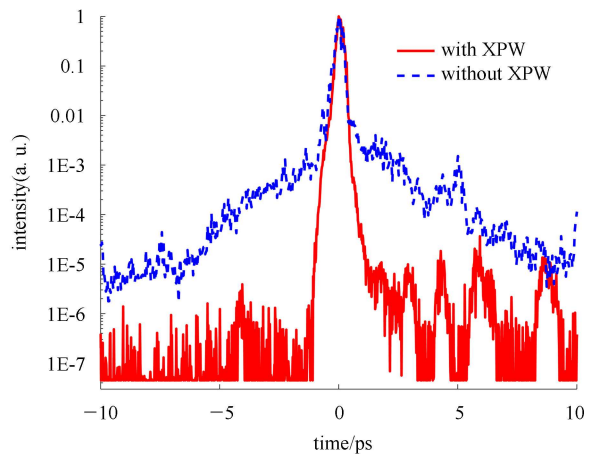


Fig. 2. (color online) Demonstration of contrast improvement when using an XPW filter. The ps contrast is measured by a third-order autocorrelator with an XPW filter (red line) and without an XPW filter (blue dashed line).

With an off-axis parabolic (OAP) mirror of 500 mm focal length (II-VI Infrared), the laser beam has been focused to near-diffraction-limited size of 16.6 μm (horizontal) and 12.3 μm (vertical) FWHM, with 50% energy enclosed in the Gaussian-fitted focal spot. The measurement is made by directly imaging the focal spot to a 10-bit CCD through a well corrected microscope objective lens. The RMS fluctuation of the focal spot position has been measured to be 2.26 μm (horizontal) and 2.65 μm (vertical), respectively, corresponding to 4–5 μrad angular pointing fluctuation.

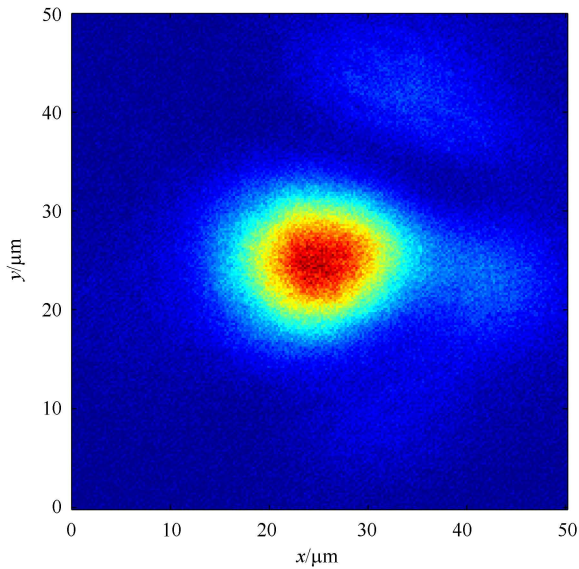


Fig. 3. The horizontal and vertical focal sizes are measured to be $16.6 \mu\text{m}$ and $12.3 \mu\text{m}$ (FWHM) with a $f=500 \text{ mm}$ OAP mirror, respectively, with the 50% energy enclosed in the Gaussian-fitted focal spot. The RMS fluctuation of the focal spot position is measured to be $2.26 \mu\text{m}$ (horizontal) and $2.65 \mu\text{m}$ (vertical), respectively.

The obtainable pulse duration of our laser system is about 60–70 fs, due to the residual high-order dispersions within the laser system. An upgrade with a new 25 fs front-end is planned later this year, and this may lead to a much shorter pulse duration.

2.2 Linear accelerator

The 45 MeV linac, as shown in Fig. 4, has two main components: a photocathode radio-frequency gun and a 3 m long S-band accelerating structure. A UV laser pulse from the TW laser system irradiates the cathode to generate an electron pulse. Solenoids are used for emittance compensation and beam envelope control. The manipulation of beam can also be achieved by a pair of quadrupole triplets. Utilizing the 20 MW RF power, the maximum electron energy can reach to 45 MeV with energy fluctuation of 1% and energy spread of 1% [14]. Several beam diagnostics have been inserted into the beam line, including beam position monitors, high-resolution YAG screens, charge detectors (Faraday cups and ICT), an S-band RF deflecting cavity [16], and an energy spectrometer.

2.3 Experimental system

The experimental system has several main components, including a vacuum interaction chamber, radiation shielding, control and data acquisition (DAQ), and plasma sources. The vacuum interaction chamber has

been properly designed to minimize the deformation during the vacuum pumping down process. Inside the chamber all of the optical components sit on a reinforced optical breadboard which is locked down to an optical table under the chamber through bellows. Fig. 5 shows the main components of the experiment station.

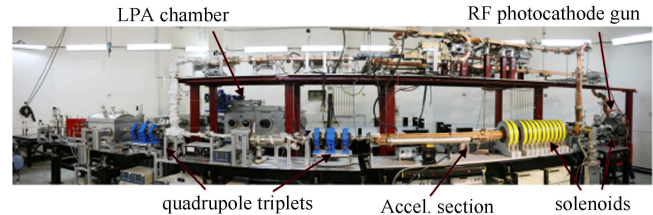


Fig. 4. The 45 MeV linac at Tsinghua University.



Fig. 5. Laser plasma experimental station.

Various gas jet nozzles of Laval type have been designed and manufactured. Gas density profiles are measured by interferometry for Argon gas. Fig. 6 shows an off-line density measurement platform and two different gas nozzles.

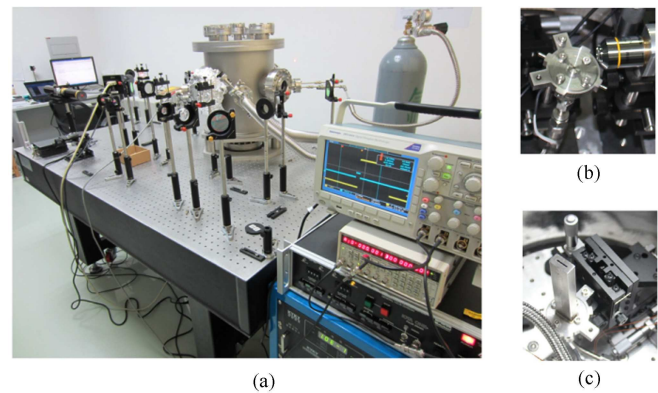


Fig. 6. Plasma source development. (a) The off-line gas density measurement platform; (b) A conical gas nozzle; (c) A $1 \text{ mm} \times 10 \text{ mm}$ slit gas nozzle.

A compact permanent magnetic spectrometer has been carefully designed to measure electron beams with a broad energy range and large momentum spread in typical laser plasma experiments. The magnet has a 15 mm

pole gap and it has a magnetic field near 1 T. Fig. 7 shows the simulated and measured data along the electron injection axis.

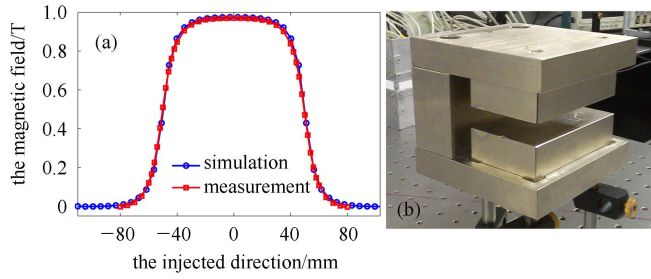


Fig. 7. The compact permanent magnetic spectrometer. (a) The designed and measured magnetic field along the electron injection axis; (b) The magnetic energy spectrometer.

3 Experimental results

Next, we present our recent experimental results on laser wakefield acceleration. Fig. 8 shows a schematic of our experimental arrangement (a) and the actual setup inside the chamber (b). After compression, the main laser pulse is sent into the interaction chamber and it is then focused close to the edge of a 2 mm-diameter helium gas jet nozzle by an OAP mirror with a focal length of 500 mm. A Mach-Zehnder interferometer combined with a delay line is set up to measure the plasma electron density profile with a probe beam split off from the main beam. Fig. 9 shows a typical interferogram at 3.3 ns delay time after the laser passes through (a) and the corresponding plasma density obtained by Abel inversion (b).

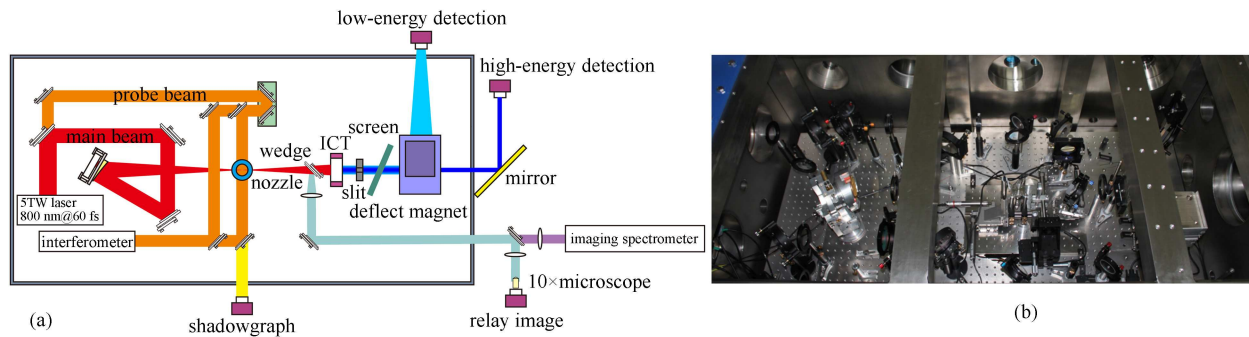


Fig. 8. A schematic of our experimental arrangement (a) and the experimental setup inside the chamber (b). The main laser pulse is sent into the interaction chamber after compression and it is then focused close to the edge of gas jet nozzle by an OAP mirror. A probe beam, split off from the main beam, is used for interferometry and shadowgraph. The electron beam spectrum, profile, and charge can be achieved by a compact magnetic spectrometer and the scintillating screens.

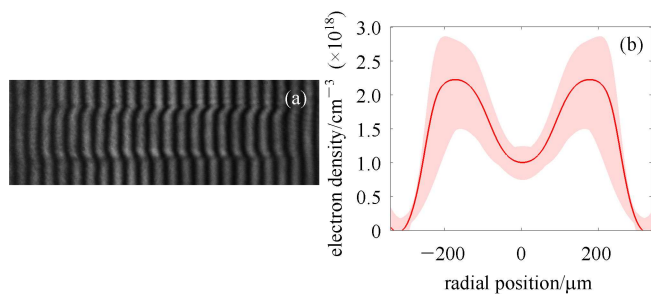


Fig. 9. Demonstration of plasma channel generation by laser ionization heating. (a) Interferometer fringes at 3.3 ns delay time after laser passing through, with a helium back pressure of 0.95 MPa; (b) The corresponding plasma density averaged over the longitudinal direction obtained by Abel inversion, which the shaded regions correspond to the standard deviation of the average over the interferogram in the longitudinal direction.

A scintillating screen (Mitsubishi: PI-200) is inserted into the beam path to simultaneously diagnose the beam profile and the beam charge. A 38 μm thick aluminum foil is placed before the screen to prevent the transmitted laser light. A magnetic spectrometer can be moved into and out of the beam path by a translation stage to measure the energy spectrum. The spectrometer is equipped with two scintillating screens on two sides to monitor the low energy and the high energy range.

By running the laser at 5 TW 60 fs, we have obtained 10–40 MeV high quality monoenergetic electron beams at a plasma density near $n_e = 5 \times 10^{19} \text{ cm}^{-3}$. Details of the measurements of the energy spectrum, the beam profile, and the beam charges are presented as follows.

3.1 Electron energy spectrum and beam profile

In the energy spectrum measurement, a 3 mm wide rectangular tungsten slit is introduced into the beam

path right before the spectrometer, which gives an uncertainty on the measured energy less than 0.2 MeV for a 25 MeV electron beam. The typical electron beam energy obtained in our experiment is in the range of 10–40 MeV. Here we show two examples. In Fig. 10(a), the electron beam has a peak energy of 25.7 MeV and a FWHM relative energy spread of 4.8%. The vertical divergence of the beam is 2.3 mrad FWHM.

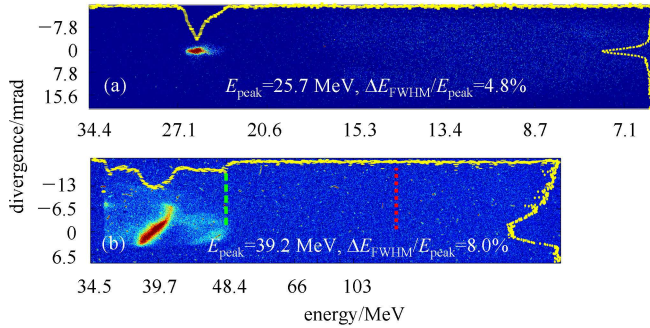


Fig. 10. Two examples of monoenergetic electron beams: (a) The peak energy of 25.7 MeV with a FWHM relative energy spread of 4.8%; (b) The peak energy of 39.2 MeV with a FWHM relative energy spread of 8%. The cut-off energy marked by the green dashed line is 49 MeV, while the laser injection position is marked by the red dotted line.

In Fig. 10(b), the electron beam has a peak energy of 39.2 MeV and a FWHM relative energy spread of 8%. The vertical divergence of the beam is 10.3 mrad FWHM. The cut-off energy of this beam is 49 MeV, as marked by the green dashed line.

A typical electron beam profile is shown in Fig. 11(a). This profile is obtained by a PI-200 screen placed 431 mm downstream of the gas jet, with a tilted angle of $(61 \pm 2)^\circ$ from the beam axis. We also put a few metal wires with different diameters right before the screen to acquire high-resolution electron radiography. Occasionally, multiple electron beams can be generated simultaneously in a single shot, an example with three different beamlets is shown in Fig. 11(b).

3.2 Charge calibration and beam charge measurement

To measure the electron beam charge accurately, we adopted a widely accepted method based on sensitive scintillating screens. Several authors provide calibration data on different scintillating screens [17, 18] using electron beams from linac. They found that two types of screens (PI-200 and Drz-high) are more sensitive than the Lanex regular screen. However, directly adopting their calibration data in our experiment may cause some

ambiguities because the exact setups and the properties of the CCD cameras are different from experiment to experiment. To avoid these ambiguities, we performed a similar calibration procedure using our in-house linac system. A relative shorter exposure time (100 μ s) is used in our calibration to reduce the background noise.

The electron beam energy of the linac is fixed at 30 MeV with a bunch duration of about 1 ps, and an ICT (Bergoz ICT-055-070-05:1) is used to benchmark the electron charge. The electron charge is kept below the saturation threshold of the scintillating screens [17]. A cooled 16-bit CCD camera (Apogee: Alta U2) with a

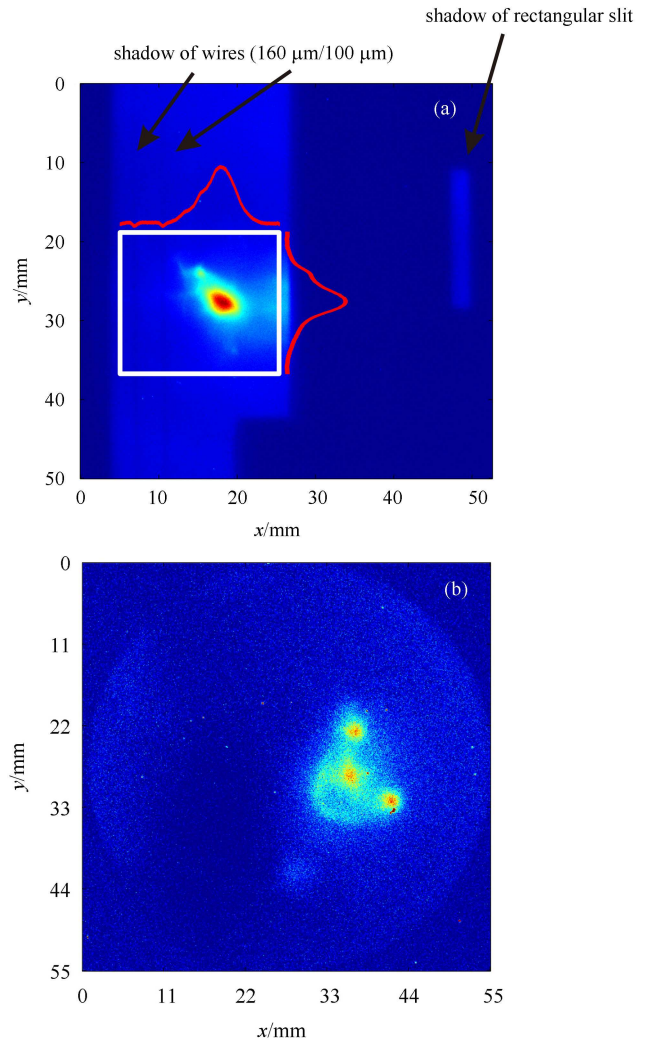


Fig. 11. Electron beam profiles on the scintillating screens: (a) The FWHM beam size with 5.53 mm (horizontal) and 4.12 mm (vertical), contributing to the average divergence of 11 mrad. The images of a rectangular slit and two metal wires (100 μ m and 160 μ m in diameter) are simultaneously produced by this accelerated beam; (b) Three different beamlets in a single shot.

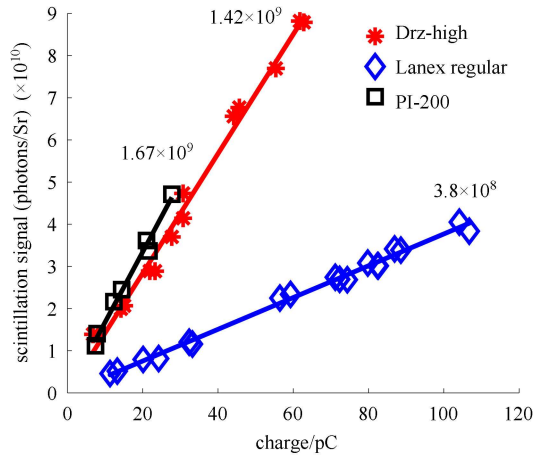


Fig. 12. Absolute charge calibration of three different screens (red for Drz-high, blue for Lanex regular and black for PI-200) using electron beams from the linac. The markers show the measured data, and the gradients of the best fit lines are also provided.

Nikon lens (focal length 60 mm and F number 1/2.8) is used to record the signal, and a band pass filter at 546 nm is applied to reduce the background light. In Fig. 12, we plot the calibration data for three different screens. We found that the PI-200 and Drz-high screens are about three times more sensitivity than Lanex Regular screen. The measured sensitivity of PI-200 is 1.67×10^9 photons/sr/pC, while the sensitivity of Drz-high is 1.42×10^9 photons/sr/pC. Based on our calibration, the charge for the electron beam shown in Fig. 11(a) is 10.6 pC, and

the charges for energy measurements are around 0.2 pC (shown in Fig. 10(a) and (b)).

4 Discussion and conclusion

A series of 3D PIC simulations using OSIRIS [19] have been performed to interpret the process of self-injection based on our experimental parameters. At the beginning, when the laser has just entered the plasma, the laser spot size is much bigger than the matched sizes [20] for given laser power and plasma density. Therefore, the laser undergoes strong self-focusing to the matched size within a few hundred microns, as shown in Fig. 13(a). Fig. 13(b) and (c) show the plasma electron distribution before and after the laser reaches the matched size. One can notice that the laser wake evolves from weakly nonlinear to the blowout/bubble structure. At the same time, injection of multiple electron bunches occurs, leading to the generation of quasi-monoenergetic electron beams. Self-guiding in the plasma wake helps to qualitatively explain the process of self-injection when run at the blow-out regime. An accurate and detailed understanding of the physics of the generation of monoenergetic electrons beams will be the subject of our future study.

A unique facility for laser plasma physics and advanced accelerator research has recently been built at Tsinghua University. This system is based on a Tsinghua Thomson scattering X-ray source (TTX), which is combined with an ultrafast TW laser with a synchronized 45 MeV high brightness linac. In our recent laser wake-field acceleration experiments, we have obtained 10–

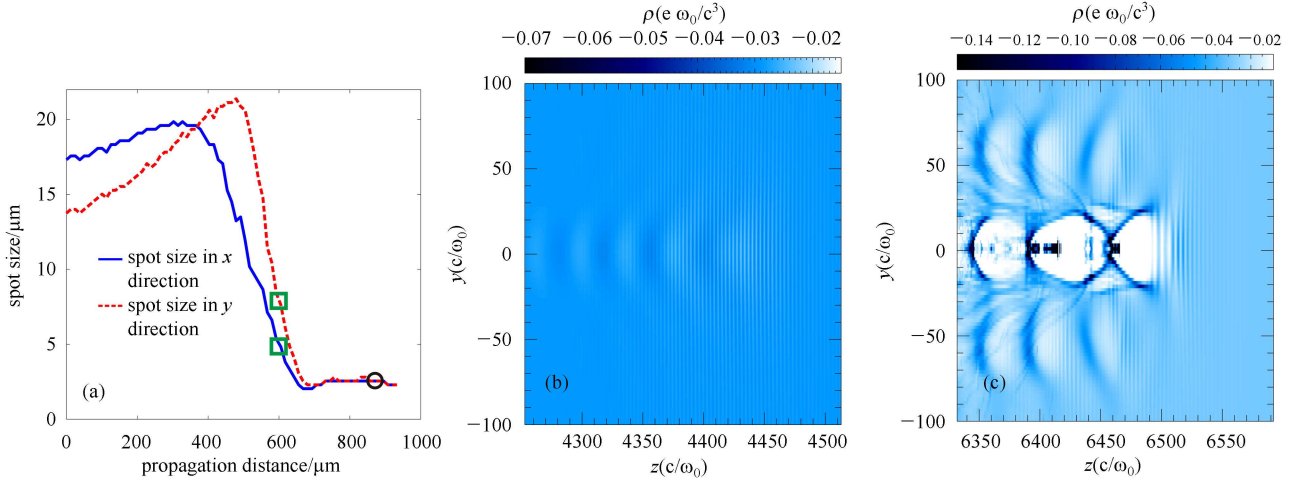


Fig. 13. 3D PIC simulation for electron self-injection using the code OSIRIS based on our experimental parameters. The laser pulse duration is 65 fs and the FWHM sizes are $16 \mu\text{m} \times 10 \mu\text{m}$ for the elliptical focal spot. The plasma density is set to $5 \times 10^{19} \text{ cm}^{-3}$ for 2 mm-long, including two 500 μm -long upramp/downramp sections. The laser beam is focused at the position of 560 μm before the plasma boundary. (a) Laser spot size evolution in two directions during the propagation in the plasma (b) Weakly non-linear structure at the position of 592 μm (marked by green square) after the laser entered the plasma. (c) Blowout/bubble structure at the position of 857 μm (marked by black circle) after the laser entered the plasma.

40 MeV high quality monoenergetic electron beams by running the laser at 5 TW peak power. Under certain conditions, very low relative energy spreads of a few percent can be achieved, which are close to the best published results [10–12]. An absolute charge calibration for three different scintillating screens has also been performed using our linac system, and the typical charge of the accelerated electron beams is in the picocoulomb range.

The authors would like to thank Dr. Z. Y. Wei, Dr. H. Teng, Dr. Z. H. Wang and Dr. J. L. Ma from Institute of Physics (CAS) for their great support on the laser system construction, Dr. J. Wang, Dr. H. -H Chu and Dr. S. -Y. Chen from National Central University (Taiwan) for their valuable information on the laser system optimization. We also thank Dr. J. Zhang from the China Institute of Atomic Energy for the use of their contrast measurement equipment.

References

- 1 Tajima T, Dawson J M. Phys. Rev. Lett., 1979, **43**: 267
- 2 Pisin Chen, Dawson J M, Robert W. Huff et al. Phys. Rev. Lett., 1985, **54**: 693
- 3 Tsung F S, Ritesh Narang, Mori W B et al. Phys. Rev. Lett., 2004, **93**: 185002
- 4 Leemans W P, Nagler B, Gonsalves A J et al. Nat. Phys., 2006, **2**: 696
- 5 Nasr A M, Hafz, Tae Moon Jeong, IL Woo ChoI et al. Nat. Photonics, 2008, **2**: 571
- 6 Clayton C E, Ralph J E, Albert F et al. Phys. Rev. Lett., 2010, **105**: 105003
- 7 LIU J S, XIA C Q, WANG W T. et al. Phys. Rev. Lett., 2011, **107**: 035001
- 8 Hyung Taek Kim, Ki Hong Pae, Hyuk Jin Cha et al. Phys. Rev. Lett., 2013, **111**: 165002
- 9 WANG Xiao-Ming, Rafal Zgadaj, Neil Fazel et al. Nat. Commun., 2013, **4**: 1988
- 10 Wiggins S M, Issac R C, Welsh G H et al. Plasma Phys. Control. Fusion, 2010, **52**: 124032
- 11 Pollock B B, Clayton C E, Ralph J E et al. Phys. Rev. Lett., 2011, **107**: 045001
- 12 Buck A, Wenz J, XU J et al. Phys. Rev. Lett., 2013, **110**: 185006
- 13 TANG Chuang-Xiang, HUANG Wen-Hui, LI Ren-Kai et al. Nucl. Instrum. Methods A, 2009, **608**: S70
- 14 DU Ying-Chao, YAN Li-Xin, HUA Jian-Fei et al. Rev. Sci. Instrum., 2013, **84**: 053301
- 15 YAN Li-Xin, DU Ying-Chao, DU Qiang et al. Chin. Phys. C (HEP & NP), 2009, **33**: 154
- 16 SHI Jia-Ru, CHEN Huai-Bi, TANG Chuang-Xiang et al. Proceedings of PAC09, 2009. 3429
- 17 Buch A, Zeil K, Popp A et al. Rev. Sci. Instrum., 2010, **81**: 033301
- 18 WU Y C, ZHU B, DONG K G et al. Rev. Sci. Instrum., 2012, **83**: 026101
- 19 Fonseca R A et al. Computational Science ICCS, 2002, **2331**: 342
- 20 LU W, HUANG C, ZHOU M, Mori W B, Katsouleas T. Phys. Rev. Lett., 2006, **96**: 165002